chemengineering

MDPI

Article

Effects of Phosphate and Thermal Treatments on the Characteristics of Activated Carbon Manufactured from Durian (*Durio zibethinus*) Peel

Astrilia Damayanti [1,*], Ria Wulansarie [1], Zuhriyan Ash Shiddieqy Bahlawan [1], Suharta [2], Mutia Royana [1], Mikhaella Wai Nostra Mannohara Basuki [1], Bayu Nugroho [1] and Ahmad Lutvi Andri [1]

[1] Department of Chemical Engineering, Faculty of Engineering E1 Building-2nd Floor, Universitas Negeri Semarang, Sekaran Campus, Gunungpati, Semarang 50229, Indonesia
[2] PT. Toya Mas Artha Prima, Ruko Griya Aviva, No.9, Jl. Menjangan Raya, Tangerang Selatan, Banten 15413, Indonesia
* Correspondence: astrilia.damayanti@mail.unnes.ac.id; Tel.: +62-85-727-155-414

Abstract: The availability of fossil energy is dwindling, so renewable fuels are the alternative choices, one of which is bioethanol. To increase the purity of the ethanol produced via the fermentation process, activated carbon (AC) was made from durian (*Durio zibethinus*) peel. The steps for making AC consist of carbonization (300 °C and 400 °C), chemical activation using phosphoric acid (10–40%), pyrolysis (700 °C and 800 °C), and neutralization. The results showed that the maximum surface area (326.72 m^2/g) was obtained from 400 °C carbonization, 800 °C pyrolysis, and activation using a 40% phosphoric acid solution. Other characteristics are the surface area of 326.72 m^2/g, pore radius of 1.04 nm, and total pore volume of 0.17 cc/g with phosphate residue in the form a P_2O_5 molecule of 3.47% by weight, with COOH, OH, CO, C=C, C=O, P-OC, and Fe-O groups with wavenumbers (cm^{-1}), respectively, of 3836, 3225, 2103, 1555, 1143, and 494. The AC also demonstrated the highest number of carbon (86.41%) upon detection using EDX, while XRF analysis verified an average carbon content of 94.45 wt%. The highest ethanol adsorption efficiency (%) and the lowest yield (%) of AC (%) were 90.01 ± 0.00 and 23.26 ± 0.01. This study shows that durian peel has great potential as the raw material for the activated carbon manufacture of ethanol adsorbents.

Keywords: characteristics; activated carbon; durian peel; carbonization; phosphoric acid; pyrolysis

check for updates

Citation: Damayanti, A.; Wulansarie, R.; Bahlawan, Z.A.S.; Suharta; Royana, M.; Basuki, M.W.N.M.; Nugroho, B.; Andri, A.L. Effects of Phosphate and Thermal Treatments on the Characteristics of Activated Carbon Manufactured from Durian (*Durio zibethinus*) Peel. *ChemEngineering* **2023**, *7*, 75. https://doi.org/10.3390/chemengineering7050075

Academic Editor: Dmitry Yu. Murzin

Received: 18 January 2023
Revised: 1 July 2023
Accepted: 15 August 2023
Published: 22 August 2023

Copyright: © 2023 by the authors. Licensee MDPI, Basel, Switzerland. This article is an open access article distributed under the terms and conditions of the Creative Commons Attribution (CC BY) license (https://creativecommons.org/licenses/by/4.0/).

1. Introduction

Significant global climate change due to greenhouse gasses generated via fossil fuel combustion has led to much research on alternative fuels that are efficient and environmentally friendly, including microbial bioethanol [1,2]. Unfortunately, the ethanol content in the broth obtained from the fermentation process is very low [3]. Meanwhile, the purity of ethanol as a biofuel is very high, which is about 99 wt% [4]. Therefore, an appropriate and energy-efficient purification technology is required, and the adsorption process using activated carbon (AC) can be a good option [5]. The research results of Downarowicz and Aleksandrzak (2017) [5] show that AC has a strong affinity for organic polar compounds, including bioethanol. Functionally, AC can also be used as a catalyst carrier [6], drinking water disinfection, energy storage, and gas storage [7].

Durian (*Durio zibethinus*) peel is a fruit waste that is known as an attractive AC precursor for its high carbon (C) content and affinity to polar compounds [8]. It is the fifth largest fruit commodity in Indonesia with around 60–75% waste of its peel [9]. The presence of lignocellulosic content in biomass requires a heating process at low and controlled temperatures in order to develop porosity in the charcoal, which is called pyrolysis/hydrothermal carbonization [10]. The hydrothermal carbonization temperature for cellulose is in the range of 300–400 °C [11] to allow complete removal of moisture and volatile compounds [10].

The production of AC via carbonization and then activation (chemical and physical) produces large amounts of carbon and expels most of the non-carbon element in gas form, which is mainly oxygen. The use of chemical activation has the advantage of transforming

the pore structure, high conversion of raw materials to carbon, and resisting the formation of tar [12]. Meanwhile, physical activation by heating at high temperatures will open carbon pores [13]. Phosphoric acid is a chemical activation agent that is widely used for large-scale synthesis of activated carbon from lignocellulosic materials because it produces high pore diameter and total volume and is relatively environmentally friendly [7].

Several studies on the carbonization temperature and activators for the manufacture of AC as adsorbents from durian peel at 400 °C with KOH and H_2SO_4 [12] and at 500 °C with KOH [14]. Unfortunately, both of them used KOH activation, which is hygroscopic [15] and leads to increased hydrophilicity of the resulting AC [16]. In addition, durian peel AC has also been studied using 10% v/v H_3PO_4 without going through carbonization, and the activation temperatures are 400 and 500 °C [17]. We know that ethanol production is still a mixture of ethanol–water, and the hydrophobicity of AC aims to allow ethanol to be adsorbed while water is retained outside of it. AC characteristics strongly depend on its pore structure which can be analyzed via surface area, volume, and pore size evaluation [18]. Other analyzes include the presence of functional groups with FTIR instruments, morphology and atomic content in AC with SEM-EDX, and chemical constituents with XRF.

In this study, AC from durian peel was manufactured via carbonization and chemical activation with phosphoric acid. The AC was characterized, its yield was optimized, and adsorption efficiency was investigated for its ability to adsorb ethanol.

2. Materials and Methods

2.1. Material Pretreatment

Durian peel was collected in Gunungpati area (Semarang City) in Central Java Province, Indonesia, and then they were cut into 6 to 8 cm. Furthermore, the raw material was dried at 70 °C until a constant weight was reached. Dried durian peel were stored in an airtight container filled with silica gel to prevent fungal growth until they were ready to be processed when needed. Commercial activated carbon (CAC) (local market) was made from coconut shells in Indonesia.

2.2. AC Synthesis

The AC was produced via carbonization (CN) process at 300 °C and 400 °C by carbonizing the durian peel in the furnace for 1 h accompanied by flowing N_2 gas at a rate of 1 L/min. Next, chemical activation was performed by soaking the carbon in various concentrations of H_3PO_4, the activator, namely 10%, 20%, 30%, and 40 wt.%, at room temperature with constant stirring at 100 rpm for 24 h. Then, the carbon was physically activated by heating it in the furnace at 700 °C and 800 °C for 1 h, accompanied by flowing N_2 gas at a rate of 1 L/min.

2.3. AC Neutralization

The AC produced was then neutralized with distilled water for 30 min at 85 °C until no longer detectable phosphor ions or other contaminants were found in the wash water, then filtered, and the filtrate was tested for its pH using a pH meter (Mettler Toledo). Washing using distilled water and 0.5 N KOH was repeated until a pH of 7 was reached. After the neutralization stage was completed, the AC was heated in an oven at 110 °C until the achievement of constant weight. Then, the AC was sieved at 8–10 mesh.

2.4. Ethanol Adsorption Test

One gram of AC was introduced into an Erlenmeyer flask containing 20 mL of 9.91% ethanol. The adsorption was carried out at room temperature with the shaker speed was 100 rpm. Ethanol samples were drawn using the same technique at 15, 30, 45, 60, and 75 min.

2.5. Determination of Ethanol Concentration

The Conway method [19] was used to determine the remaining ethanol content after being adsorbed with AC. The Conway cup containing 3 mL of dichromic acid, 0.5 mL of ethanol after adsorption, and 1 mL of 20% Na_2CO_3 was placed in the oven at 90 °C for 20 min before cooling back to room temperature. The dichromic acid in the Conway cup was diluted to 25 mL, and the absorbance was measured using a UV Vis Spectrophotometer (Genesys 10) with a maximum wavelength of 444 nm. Then, the absorbance value obtained was substituted for the linear equation resulting from the ethanol calibration curve to determine the ethanol concentration resulting from adsorption. AC adsorption of durian peel compared to CAC.

2.6. Determination of Ethanol Adsorption Efficiency via AC

The adsorption efficiency via AC in this study was calculated using Equation (1) [20].

$$\%\ adsorption\ efficiency = \frac{C_0 - C_t}{C_0} \times 100\% \quad (1)$$

where C_0 and C_t refer to concentration of ethanol solution (%) before and after the adsorption process

2.7. Determination of Yield of AC

The yield of AC in this study was calculated using Equation (2) [21].

$$\text{yield of AC } (\%) = \frac{\text{AC}}{\text{C}} \times 100\% \quad (2)$$

where AC and C refer to total mass (g) of activated carbon and carbon

2.8. Characterizations of AC and CAC before and after Activation

The surface area, pore volume, and pore diameter were quantified using nitrogen adsorption–desorption (Brunauer–Emmett–Teller, BET) model Nova 1200 e, Quantachrome). The pore size distribution is obtained from the desorption branch of the hysteretic adsorption isotherm. Functional groups were analyzed using Fourier Transform Infrared Spectroscopy (FTIR) model Perkin Elmer Spectrum IR 10.6.1. (PerkinElmer, Waltham, MA, USA) Scanning Electron Microscope–Energy Dispersive X-ray (SEM-EDX) model SEM-EDX JEOL JSM-6510LA (JEOL, Showima City, Tokyo, Japan) was used to study surface chemistry and pore structure (SEM) and atomic content (EDX, Thermo Fisher Scientific, Waltham, MA, USA). Prior to SEM analysis, the sample was coated with thin layer of gold and then mounted to a puncture made of copper with the help of carbon double-sided tape. Meanwhile, the elemental composition of the AC was analyzed via EDX. Determination of the chemical constituents of AC was evaluated using X-ray Fluorescence (XRF) Spectrometry (Wavelength Dispersive X-ray Fluorescence (WDXRF) model Rigaku Supermini200, Quantachrome TouchWin ver. 1.11, Rigaku, The Woodlands, TX, USA).

3. Results and Discussion

3.1. Surface Area of AC of Durian Peel

The results of BET analysis with thermal CN 300 and 400 °C at various concentrations of phosphoric acid at pyrolysis temperatures of 700 °C and 800 °C are presented in Tables 1 and 2. Accordingly, the surface area comparison of the ACs obtained from this study and CAC is shown in Table 3.

Table 1 shows that the CA samples activated with 40% H_3PO_4 exhibit a larger surface area and is most compared to other concentrations in the same CN and pyrolysis temperature group. The results of the BET analysis in this study agreed well with those reported by [22,23], where CAs activated with H_3PO_4 possessed a surface area of 16, 56.78, and 257.50 m^2/g, respectively.

Table 1. BET result of AC pyrolized at 700 °C.

Sample	Surface Area (m^2/g)	Pore Size (Å)	Pore Volume (cc/g)
AC700-300-10%	51.1	19.5	0.05
AC 700-300-20%	37.5	15.6	0.03
AC 700-300-30%	81.0	15.6	0.04
AC 700-300-40%	259	16.7	0.04
AC 700-400-10%	16.3	15.7	0.02
AC 700-400-20%	35.8	15.7	0.04
AC 700-400-30%	51.5	15.7	0.04
AC 700-400-40%	102	15.6	0.04

Table 2. BET result of AC pyrolized at 800 °C.

Sample	Surface Area (m^2/g)	Pore Size (Å)	Pore Volume (cc/g)
AC 800-300-10%	2.81	15.2	0.002
AC 800-300-20%	67.2	13.2	0.044
AC 800-300-30%	258	11.1	0.14
AC 800-300-40%	292	11.6	0.16
AC 800-400-10%	2.09	16.4	0.003
AC 800-400-20%	216	10.2	0.11
AC 800-400-30%	254	10.3	0.13
AC 800-400-40%	327	10.4	0.17

Table 3. Surface area comparison of this study and CAC.

Sample		Surface Area (m^2/g)
Before Activation	CN300	51.738
After Activation	AC 700-300-40%	259.243
	AC 800-300-40%	291.64
Before Activation	K400	49.460
After Activation	AC 700-400-40%	101.897
	AC 800-400-40%	326.72
CAC		50.374

Table 2 shows that the CN temperature of 400 °C produces a higher surface area (326.72 m^2/g) than 300 °C (291.64 m^2/g). Indeed, raising the activator concentration while also raising the surface area and pore volume can be seen in Tables 1 and 2. It is due to the intensive interaction between the phosphoric acid molecules and the carbon structure. So, the carbon decomposes into cellulose to form phosphates oxide (P_2O_5), which forms pores [24]. The pore size decreased sharply as the activator concentration increased from 10% to 20%. However, the reduction in pore size was not significant at activator concentrations exceeding 20%. It is due to the lower the volatile matter content, the smaller the pore diameter [25]. The increase in pore volume is to have a good effect on adsorption because it can provide optimal adsorption space in AC [26].

The increase in surface area (Table 3) occurs as activation temperature, pyrolysis temperature, and H_3PO_4 concentration increase. The best results were when the pyrolysis, activation, and H_3PO_4 concentration conditions were AC800-400-40%, which reached about 6.6 times the increase in surface area after activation. It is also the same as the results of the SEM-EDX test, where AC 800-400-40% has the most wrinkles, so it has a large surface area.

In contrast, the AC obtained from AC700-400-10% has a small surface area, consists of fragments, and is less porous. It is presumably due to variations in temperature conditions during pyrolysis that aims for thermal decomposition [27]. So, the higher the pyrolysis temperature, the more open pores there are, but the yield will decrease [28]. Several studies on the effect of using phosphoric acid activation on yield and surface area in the manufacture of AC with biomass precursors are presented in Table 4.

Table 4. Several studies on the effects of using phosphoric acid activation on yield and surface area in the manufacture of AC with biomass precursors.

Precursors	Aqueous Solution with Concentration	Impregnation Ratio H_3PO_4 to Sample	CN and Activation Temperature (°C)	Adsorbate	Yield (%)	BET Surface Area (m^2/g)	References
Durian peel	85 wt.%	3:1–6:1 ± α	Activation = 400–600 ± α	NH_3-N	21.02	906.48 at 400 °C	[29]
Durian peel	85 wt.%	3:1–6:1 ± α	Activation = 400–600 ± α	NH_3-N and COD	N.A	906.48	[30]
Durian shell	1 M	25:1	CN 250–350 Activation = 400–700	N.A	N.A	2004	[31]
Durian shell	5,10,20,30, 50%	0.7, 1.4, 2.8, 4.2, 8.4	CN = 500	toluene	N.A	1404 at 30%	[32]
Durian seed	85 wt.%	1:1–6:1	Activation = 600 and 900	N_2	46.82	2123 at 600 °C	[33]
Durian seed (50%) and rambutan peels (50%)		each as much as 1 g to 2 mL H_3PO_4	Activation = 100	N_2	N.A	104.2	[34]
Durian peel	10% *v*/*v* overnight	1:1.4	Activation = 400 and 500	N.A	63	1024 at 500 °C	[17]
Coconut shell	20, 30, 40, 50 wt.%	3.5:1	CN 400–600	methylene blue	36.9	891	[35]
Rice husk	40–85 wt.%	3:1–6:1	Activation = 300–600	N.A	44.6	1820	[36]
Rice husk	40–85 wt.%	3:1–6:1	Activation = 300–600	N.A	44.6	1820	[36]
Palm shell	65 wt.%	1.75:1	Activation = 375, 425, 475, and 525	N.A	55	1109	[37]
Durian Peel (This study)	10–40 wt.%	6:1	CN 300–400 Activation = 700–800	ethanol	49.67% for 700-300-40%	326.72 for 800-400-40%	

3.2. FTIR Analysis

The results of the FTIR analysis of the AC's surface with concentrations of 10%, 20%, 30%, and 40% are shown in Figure 1.

The wavenumber of 2500–3500 cm^{-1} characterizes the steepest and dominant number of −OH compared to other functional groups in both the same and different treatments (Figure 1) so that the AC has a hydrophilic site [38].

The detected vibrations 3839–3567 cm^{-1} were obtained from the -COOH functional group in the variables AC 800-400-20%, AC 800-400-30%, AC 800-400-40%, AC 700–300, and AC 700-400-20% (Figure 1). Meanwhile, the wavenumber of 3262–3225 cm^{-1} indicates the presence of the −OH functional group of the hydroxyl group [39]. The wavenumber 2263–2261 cm^{-1} is the C≡C vibration of the alkyne group [40] and was only found in the variables AC 800-300-10%, AC 800-400-10%, AC 800-300-20%, and AC 800-300-30%. Conversely, the C=C stretching disappeared at a concentrated activator concentration of 40%, indicating that many weak bonds disappeared in the activation process [41]. Based on Thue et al. 2017 [42], the discovery of carbonyl (C=O) and hydroxyl (−OH) on AC will reduce hydrophobicity because these functional groups easily bind water.

An aromatic bond C=C is found at a peak between 1532 and 1623 cm^{-1}, which is more stable at a higher pyrolysis temperature [40]. The stretching vibrations of the P-OR functional group of esters with the weak band had been found at peaks of 876 cm^{-1} at AC 800-300-40%, 932 cm^{-1} at AC 800-400-30%, and 933 cm^{-1} at AC 800-400-20% [43]. The accumulation of Fe atoms on activated carbon was indicated by the Fe-O stretching vibrations found in all variables AC800-400-(10–40%) between 488 and 536 cm^{-1} [44]. A strong band at approximately 1058–1177 cm^{-1} as a result of the activation process with H_3PO_4 produces char oxidation, introducing oxygenated functionalities in the AC, was probably the stretching of the O–C bond in the P–O–C linkage (aromatic bond) or hydrogen-bonded P=O in a phosphate ester [37].

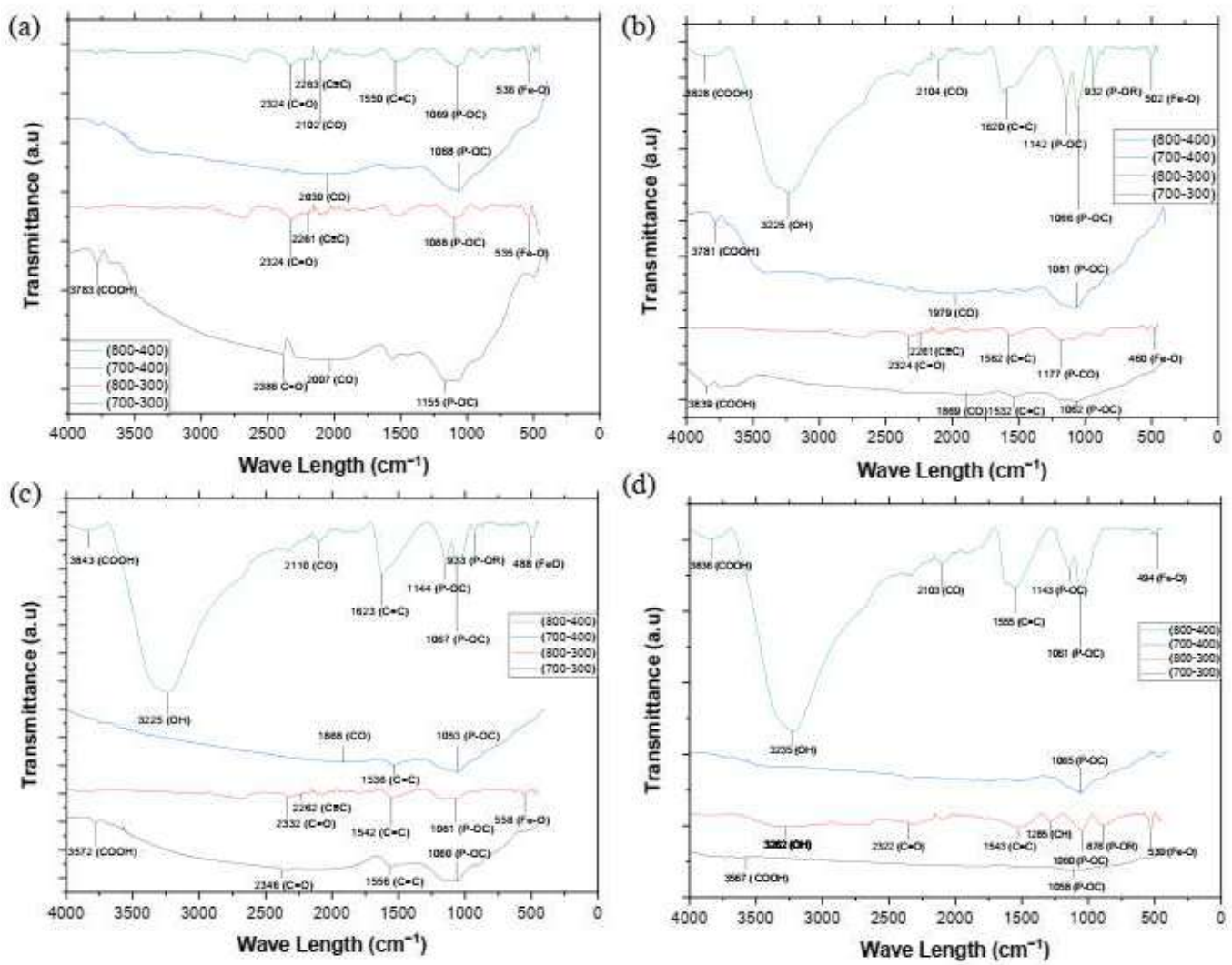

Figure 1. Comparison of FTIR AC at concentration H_3PO_4 of (**a**) 10%, (**b**) 20%, (**c**) 30%, and (**d**) 40%.

3.3. XRF Analysis

The chemical compositions of CN and AC were analyzed using XRF [41], with the results presented in Tables 5–9. Several inorganic species, such as K_2O, P_2O5, SiO_2, CaO, and Fe_2O_3, are present in durian peel and can be considered impurities. The concentration of these impurities increased with the CN temperature [45].

The mass percentage of component C in CN300 (97.5) is more than in CN400 (96.2) (Table 5) because the CN temperature of 400 C is higher than 300 C, so the release of volatile compounds is complete [45].

Table 5. Chemical components of CN temperature.

Component	CN300	CN400
C	97.5	96.2
P_2O_5	0.19	0.33
SiO_2	0.25	0.27
Fe_2O_3	0.01	0.01
K_2O	1.69	2.73
CaO	0.22	0.20

Table 6. Chemical components of AC 700–300.

Component	Variable Composition (wt.%)			
	10%	**20%**	**30%**	**40%**
C	91.8	92.4	92.5	92.9
P_2O_5	5.60	5.32	4.86	4.86
SiO_2	0.22	0.21	0.21	0.24
Fe_2O_3	0.02	0.02	0.03	0.17
K_2O	2.17	1.69	2.04	1.54
CaO	0.16	0.29	0.17	0.14

Table 7. Chemical components of AC 700–400.

Component	Variable Composition (wt.%)			
	10%	**20%**	**30%**	**40%**
C	91.7	94.1	91.7	92.1
P_2O_5	5.50	5.12	5.36	5.01
SiO_2	0.32	0.22	0.28	0.24
Fe_2O_3	0.02	0.03	0.03	0.15
K_2O	2.05	0.19	2.27	2.16
CaO	0.23	0.13	0.15	0.14

Table 8. Chemical components of AC 800–300.

Component	Variable Composition (wt.%)			
	10%	**20%**	**30%**	**40%**
C	93.9	93.3	94.0	94.0
P_2O_5	5.03	5.12	4.62	4.71
SiO_2	0.28	0.20	0.19	0.22
Fe_2O_3	0.01	0.01	0.01	0.02
K_2O	0.66	1.27	1.03	0.87
CaO	0.13	0.11	0.09	0.11

Table 9. Chemical components of AC 800–400.

Component	Variable Composition (wt.%)			
	10%	**20%**	**30%**	**40%**
C	96.8	97.1	93.6	94.9
P_2O_5	4.84	4.03	4.61	3.47
SiO_2	0.26	0.200	0.21	0.16
Fe_2O_3	0.02	0.03	0.35	0.06
K_2O	0.90	1.17	0.97	1.30
CaO	0.16	0.09	0.10	0.08

Tables 6–9 have in common the components of AC from largest to smallest, namely C (more than 91%), P_2O_5, and K_2O. The carbon content after pyrolysis is lower than after CN. It may be due to the many carbon bonds removed at an average of 3–4 wt.%. However, the content of compound C in the variables AC800-400-10% and AC800-400-20% (Table 9) is higher than CN400 (Table 5). Increasing the pyrolysis temperature enriches the carbon content in the AC by removing non-carbon species. However, an increase in the concentration of H_3PO_4, especially 30 and 40%, reduced the carbon content, presumably due to the partial gasification of the carbon via P_2O_5 and volatilization of phosphorus compounds. Meanwhile, thermal pyrolysis $\geq$400 °C produces P_2O_5 due to the decomposition of H_3PO_4, and inorganic substances have active components despite low chemical reaction ability, such as silica (SiO_2), Fe_2O_3, K_2O, and CaO. The following is a sequence of amorphous SiO_2 (crystalline silica): AC700–400 (Table 7) > AC700–300 (Table 6) > AC800–400 (Table 9) > AC800–300 (Table 8).

In contrast, as the phosphoric acid concentration increases, the SiO_2 content tends to decrease [46].

On the other hand, the chemical composition of AC carbonized at 400 °C is higher than at 300 °C because the deformation of complex chemical compounds becomes simpler than at pyrolysis temperatures of 700 °C and 800 °C, so many compounds with new bonds form [47].

3.4. SEM-EDX Analysis

The surface morphologies of C (Figure 2), AC (Figure 3) and CAC (Figure 4) were observed using SEM. Meanwhile, the atomic content of carbon, AC, and CAC are presented in Figures 5–7, respectively.

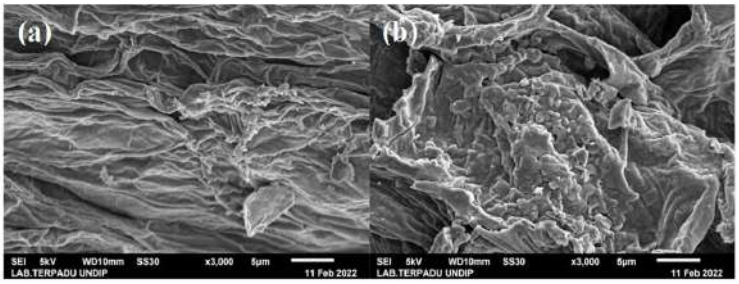

Figure 2. Surface morphology of C on CN variable (magnification ×3000) (**a**) 300 °C and (**b**) 400 °C.

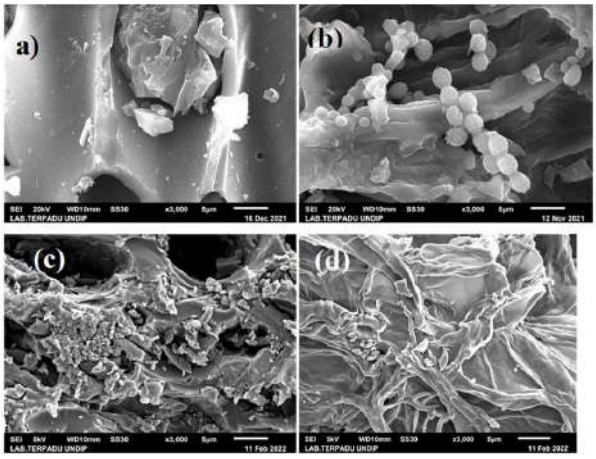

Figure 3. Surface morphology of AC (×3000) with 40% phosphoric acid concentration: (**a**) AC700-300, (**b**) AC700-400, (**c**) AC800-300, and (**d**) AC800-400.

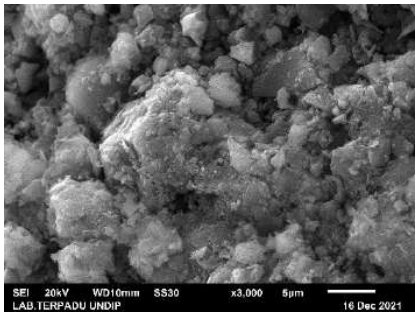

Figure 4. Morphology of CAC.

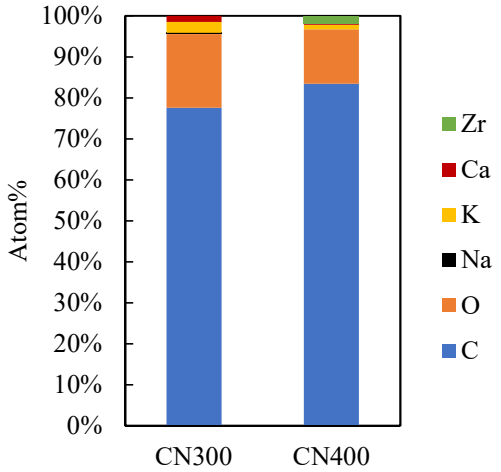

Figure 5. Atomic content in carbonization variables.

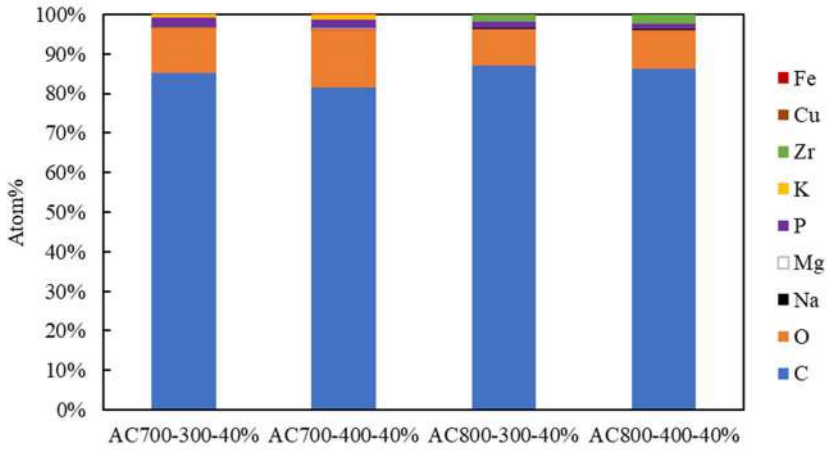

Figure 6. Atomic content (%) of AC using 40% phosphoric acid in CN and pyrolysis variables.

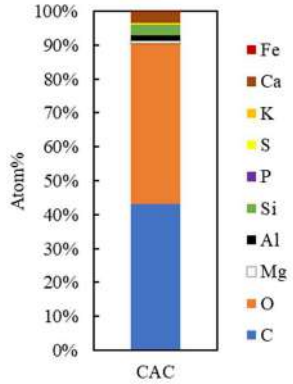

Figure 7. Atomic content of CAC.

The morphology of the durian peel carbonized at 300 °C showed a wrinkled carbon surface without the pores because the durian peel carbon has not been able to decompose the volatile content [48,49]. On the other hand, the durian peel C at 400 °C (Figure 2b) showed pores starting to form but not evenly distributed over the entire C surface due to good pore structure as temperature increases [48,50].

All the variables shown in Figure 3 have a morphology in which many tunnel-like pores are formed on the surface of the AC. However, AC pyrolysis at 700 °C and 800 °C tends to produce the morphology of fragments and wrinkles. Figure 3 shows the pore

volume of the SEM images, which is wider with higher CN and pyrolysis temperatures. Figure 3a shows a blockage in the pores in the form of C loss, which is thought to be due to the activation process. The appearance of a small spherical shape that sticks around the pores (Figure 3b) is thought to be residual KOH when the AC was neutralized.

The significant difference between the morphology of AC (Figure 3) and C (Figure 2) is the formation of porosity as a result of the activation of phosphoric acid on carbon to produce new products in the form of phosphate esters and polyphosphates [24].

Figure 4 shows forming many narrow fissure structures [35].

Figure 5 shows that the carbon content increases with increasing temperature. On the other hand, oxygen is decreasing. In addition, increasing the temperature also produces Zr.

After C was activated (Figure 6), new atoms appeared, namely Fe, P, Cu, and Mg. Figure 6 showed that C, O, and phosphorus (P) were the dominant compounds in the AC produced. The number of C atoms (%) produced from AC700-300-40%, AC700-400-40%, AC800-300-40%, and AC800-400-40%, respectively, are 85.14, 81.55, 86.88, and 86.14. The presence of P in AC is due to the availability of the phosphoric acid activator [51]. that helps the adsorbent to increase the hydrophobic properties of C [52]. AC. with a pyrolysis temperature of 800 °C, has a higher C content and a lower O content than 700 °C due to the organic matter's contaminants, which prevented the N_2 from removing them during the carbon synthesis process and resulted in poor product qualities [48].

The low C content (~42%) in CAC (Figure 7). In addition, the levels of O, P, K, and Mg in CAC are similar to the results of previous studies [53]. The Mg, aluminum (Al), and ferrum (Fe) atoms in Figure 6 are due to be ashes in the activated carbon, which are considered impurities and unnecessary trace amounts of elements like Fe, Si, Mn, and Ca that are frequently found in coconut shells. Chemicals like P and K are also available for activation procedures [54].

3.5. Effect of Temperature on Various Pyrolysis, CN, and H_3PO_4 Concentrations on Adsorption Efficiency via AC

The relevant adsorption efficiency measurements taken at various pyrolysis and CN temperature ranges are shown in Table 10. The concentration of phosphoric acid caused noticeable changes to be found.

Table 10. Effect of temperature on various pyrolysis, CN, and H_3PO_4 concentrations on AC adsorption efficiency.

Temperature (°C)		Adsorption Efficiency (%)			
Pyrolysis	**CN**	**10%**	**20%**	**30%**	**40%**
700	300	86.17 ± 0.41	50.36 ± 0.20	53.61 ± 0.00	79.66 ± 0.20
	400	81.28 ± 0.00	41.00 ± 0.00	77.21 ± 0.00	56.87 ± 0.20
800	300	89.82 ± 0.20	89.71 ± 0.06	89.85 ± 0.02	89.83 ± 0.20
	400	89.74 ± 0.06	89.76 ± 0.21	89.82 ± 0.40	90.01 ± 0.00

Table 10 shows the adsorption efficiency calculated using Equation (3) that the highest efficiencies have AC800-400-40% (90.01%). It is suspected that nearly all of the ethanol can be adsorbed via the activated carbon. The AC adsorption efficiency increases with the pyrolysis temperature. It has proven that the adsorption efficiency of AC at AC800-300 and AC800-400 is higher than pyrolysis at 700 °C. On the other hand, the decrease in its efficiency is due to the adsorption sites on AC being covered by adsorbate particles, causing a reduction in the total surface area and inhibiting the adsorption process [55].

Table 10 shows the fluctuating adsorption efficiency at AC700-300°C, namely 86.17%, 50.36%, 53.61%, and 79.66% for H_3PO_4 concentrations of 10%, 20%, 30%, and 40%, respectively. It is due to the excessive cross-linking reaction between C-O-P during the impregnation process [52]. A similar phenomenon also occurs at AC700-400 °C, where the adsorption efficiency was the highest for 10% H_3PO_4, but a fluctuating adsorption

efficiency is obtained for 20–40% H_3PO_4. It is due to the cross-linking of biopolymers from phosphate esters, and polyphosphates are a new product resulting from the activation of phosphoric acid, which expands porosity. Nevertheless, the excessive concentrations of phosphoric acid form an insulating layer on the surface of the AC, thereby inhibiting ethanol adsorption [24]. On the other hand, the higher the CN temperature treatment and activation, the more the insulating layer on the AC surface disappears, so the ethanol adsorption is also higher.

3.6. Effect of Temperature on Various Pyrolysis, CN, and H_3PO_4 Concentrations on Yield of AC

The effect of pyrolysis temperature, CN temperature, and H_3PO_4 concentrations on the yield of AC is shown in Table 11.

Table 11. Effect of pyrolysis temperature, CN temperature, and H_3PO_4 concentrations on the yield of AC.

Temperature (°C)		Yield (%)			
Pyrolysis	**CN**	**10%**	**20%**	**30%**	**40%**
700	300	32.46 ± 0.1	37.56 ± 0.08	42.06 ± 0.05	49.67 ± 0.03
	400	31.85 ± 0.01	36.33 ± 0.02	40.61 ± 0.05	46.80 ± 0.06
800	300	30.62 ± 0.05	32.33 ± 0.1	33.34 ± 0.05	35.07 ± 0.06
	400	21.10 ± 0.2	21.98 ± 0.03	22.51 ± 0.06	23.26 ± 0.01

Table 11 shows that as the concentration of H_3PO_4 increases, the yield of AC decreases. The mechanism of pore formation begins with a reaction in the form of dehydration, degradation, and coagulation changes between phosphoric acid and hemicellulose and lignin contained in carbon which causes the formation of aliphatic structures. The process is continued by heating the AC to high temperatures to form phosphate ester bonds and polyphosphate ester bonds. Then, when the temperature is above 600 °C, the compounds H_3PO_4, $H_2PO_4{}^{-1}$, and $H_2P_2O_7{}^{-2}$ can evaporate, causing the phosphate ester and polyphosphate bonds to break in the precursor matrix. As a result, many new pores are formed [56,57]. The results of this study are similar to previous studies [56–58].

A comparison of adsorption efficiency and yield of AC from biomass is presented in Table 12.

Table 12. Comparison of adsorption efficiency and yield of AC from biomass precursors using phosphoric acid activation.

Precursor	Activating Agent	Carbonization and Activation Temperature (°C)	Yield (%)	Adsorbate	Highest Adsorption Efficiency (%)	References
Durian Peel	H_3PO_4 30%	Activation: 600	86.90	-	-	[51].
Banana Peel	H_3PO_4 25%	CN: 470	73.83	-	-	[47]
Durian Peel	-	CN: 250	-	COD Removal	68.65	[59]
Eucalyptus Residue	H_3PO_4 40%	Activation: 300–600	54.3 for 300 °C	Methylene Blue Solution	99.6	[51]
Mangrove Pile Leftover	H_3PO_4	Activation: 300–500	44.7 for 300 °C	Methylene Blue Solution	96.3 for 300 °C	[60]
Periwinkle Shell	H_3PO_4 (0.5M)	Activation: 700	-	Cyanide Removal	76.6	[61]
Durian Peel	H_3PO_4 10–40%	CN: 300–400 Activation: 700–800	49.67 for 700-300-40%	Ethanol	90.01 for 800-400-40%	This study

4. Conclusions

The sequence of AC manufacturing stages from durian peel for bioethanol purification consists of CN (300–400 °C), the activation of H_3PO_4 (10–40%), pyrolysis (700–800 °C), and neutralization. The best results were characterized via carbonization at 400 °C, activator concentration at 40% H_3PO_4, and pyrolysis at 800 °C as follows: surface area of 326.72 m^2/g, pore radius of 1.04 nm, and total pore volume of 0.17 cc/g with phosphate residue in the form a P_2O_5 molecule of 3.47% by weight, with COOH, OH, CO, C=C, C=O, P-OC, and

Fe-O groups with a wavenumber (cm^{-1}), respectively, are 3836, 3225, 2103, 1555, 1143, and 494 as well as XRF with phosphate residue (P_2O_5), which is 3.47% by weight. The AC also demonstrated the highest amount of carbon (86.41% by mass), while the adsorption efficiency (%) of bioethanol and yield (%) of AC were 90.01 ± 0.00 and 23.26 ± 0.01. The surface area of AC from durian peel was 6.5 times larger than CAC derived from coconut shells.

Author Contributions: Writing—original draft, A.D. and S.; data curation, formal analysis, M.R., M.W.N.M.B., B.N. and A.L.A.; supervision, resources, methodology, Z.A.S.B.; project administration, supervision, investigation, R.W.; writing—review and editing, A.D. All authors have read and agreed to the published version of the manuscript.

Funding: This research was funded by Universitas Negeri Semarang through a research grant under a contract of DIPA UNNES No. 57.8.4/UN37/PPK.3.1/2022.

Data Availability Statement: Data available on request.

Acknowledgments: The authors gratefully acknowledge the financial support from Universitas Negeri Semarang through a research grant under a contract of DIPA UNNES No. 57.8.4/UN37/PPK.3.1/2022. The authors also thank A. C. Kumoro from Universitas Diponegoro for the discussion of the experimental results.

Conflicts of Interest: The authors declare no conflict of interest.

References

1. Rastogi, M.; Shrivastava, S. Recent Advances in Second Generation Bioethanol Production: An Insight to Pretreatment, Saccharification and Fermentation Processes. *Renew. Sustain. Energy Rev.* **2017**, *80*, 330–340. [CrossRef]
2. Kumoro, A.C.; Damayanti, A.; Bahlawan, Z.A.S.; Melina, M.; Puspawati, H. Bioethanol Production from Oil Palm Empty Fruit Bunches Using Saccharomyces Cerevisiae Immobilized on Sodium Alginate Beads. *Period. Polytech. Chem. Eng.* **2021**, *65*, 493–504. [CrossRef]
3. Achinas, S.; Euverink, G.J.W. Consolidated Briefing of Biochemical Ethanol Production from Lignocellulosic Biomass. *Electron. J. Biotechnol.* **2016**, *23*, 44–53. [CrossRef]
4. Karimi, S.; Karri, R.R.; Tavakkoli Yaraki, M.; Koduru, J.R. Processes and Separation Technologies for the Production of Fuel-Grade Bioethanol: A Review. *Environ. Chem. Lett.* **2021**, *19*, 2873–2890. [CrossRef]
5. Downarowicz, D.; Aleksandrzak, T. Isobutanol Vapor Adsorption on Activated Carbons: Equilibrium and Kinetic Studies. *J. Chem. Eng. Data* **2017**, *62*, 3518–3524. [CrossRef]
6. Sharma, G.; Sharma, S.; Kumar, A.; Lai, C.W.; Naushad, M.; Shehnaz; Iqbal, J.; Stadler, F.J. Activated Carbon as Superadsorbent and Sustainable Material for Diverse Applications. *Adsorpt. Sci. Technol.* **2022**, *2022*, 4184809. [CrossRef]
7. Neme, I.; Gonfa, G.; Masi, C. Activated Carbon from Biomass Precursors Using Phosphoric Acid: A Review. *Heliyon* **2022**, *8*, e11940. [CrossRef]
8. Miskah, S.; Aprianti, T.; Agustien, M.; Utama, Y.; Said, M. Purification of Used Cooking Oil Using Activated Carbon Adsorbent from Durian Peel. *IOP Conf. Ser. Earth Environ. Sci.* **2019**, *396*, 012003. [CrossRef]
9. Kumoro, A.C.; Alhanif, M.; Wardhani, D.H. A Critical Review on Tropical Fruits Seeds as Prospective Sources of Nutritional and Bioactive Compounds for Functional Foods Development: A Case of Indonesian Exotic Fruits. *Int. J. Food Sci.* **2020**, *2020*, 4051475. [CrossRef]
10. MacDermid-Watts, K.; Pradhan, R.; Dutta, A. Catalytic Hydrothermal Carbonization Treatment of Biomass for Enhanced Activated Carbon: A Review. *Waste Biomass Valorization* **2021**, *12*, 2171–2186. [CrossRef]
11. Li, J.; Zhao, P.; Li, T.; Lei, M.; Yan, W.; Ge, S. Pyrolysis Behavior of Hydrochar from Hydrothermal Carbonization of Pinewood Sawdust. *J. Anal. Appl. Pyrolysis* **2020**, *146*, 104771. [CrossRef]
12. Sriprom, P.; Krusong, W.; Assawasaengrat, P. Preparation of Activated Carbon from Durian Rind with Difference Activations and Its Optimization. *J. Renew. Mater.* **2020**, *9*, 311–324. [CrossRef]
13. Hassan, M.F.; Sabri, M.A.; Fazal, H.; Hafeez, A.; Shezad, N.; Hussain, M. Recent Trends in Activated Carbon Fibers Production from Various Precursors and Applications—A Comparative Review. *J. Anal. Appl. Pyrolysis* **2020**, *145*, 104715. [CrossRef]
14. Legiso, L.; Susanto, T.; Roni, K.A.; Ramadhan, M.B.; Lestari, D.W.; Farida, F. Activation of Activated Carbon from Durian Peel as A Waste Adsorbent from Laundry Activities. *Maj. BIAM* **2020**, *16*, 58–63. [CrossRef]
15. Chen, W.; Wang, X.; Hashisho, Z.; Feizbakhshan, M.; Shariaty, P.; Niknaddaf, S.; Zhou, X. Template-Free and Fast One-Step Synthesis from Enzymatic Hydrolysis Lignin to Hierarchical Porous Carbon for CO_2 Capture. *Microporous Mesoporous Mater.* **2019**, *280*, 57–65. [CrossRef]
16. Li, K.; Zhou, M.; Liang, L.; Jiang, L.; Wang, W. Ultrahigh-Surface-Area Activated Carbon Aerogels Derived from Glucose for High-Performance Organic Pollutants Adsorption. *J. Colloid. Interface Sci.* **2019**, *546*, 333–343. [CrossRef] [PubMed]

17. ThamYee, J.; Arumugam, S.D.; Nur Hidayah, A.L.; Abdullah, A.M.; Latif, P.A. Effect of Activation Temperature and Heating Duration on Physical Characteristics of Activated Carbon Prepared from Agriculture Waste. *Environ. Asia* **2010**, *3*, 143–148.
18. Lillo-Ródenas, M.A.; Cazorla-Amorós, D.; Linares-Solano, A. Behaviour of Activated Carbons with Different Pore Size Distributions and Surface Oxygen Groups for Benzene and Toluene Adsorption at Low Concentrations. *Carbon. N. Y.* **2005**, *43*, 1758–1767. [CrossRef]
19. Sriariyanun, M.; Mutrakulcharoen, P.; Tepaamorndech, S.; Cheenkachorn, K.; Rattanaporn, K. A Rapid Spectrophotometric Method for Quantitative Determination of Ethanol in Fermentation Products. *Orient. J. Chem.* **2019**, *35*, 744–750. [CrossRef]
20. Alghamdi, A.A.; Al-Odayni, A.-B.; Saeed, W.S.; Al-Kahtani, A.; Alharthi, F.A.; Aouak, T. Efficient Adsorption of Lead (II) from Aqueous Phase Solutions Using Polypyrrole-Based Activated Carbon. *Materials* **2019**, *12*, 2020. [CrossRef]
21. Sriatun, S.; Herawati, S.; Aisyah, I. Effect of Activator Type on Activated Carbon Characters from Teak Wood and The Bleaching Test for Waste Cooking Oil. *J. Rekayasa Kim. Lingkung.* **2020**, *15*, 79–89. [CrossRef]
22. Kumari, G.; Soni, B.; Karmee, S.K. Synthesis of Activated Carbon from Groundnut Shell Via Chemical Activation. *JIEIE* **2022**, *103*, 15–22. [CrossRef]
23. Wan Mahmood, W.N.; Samsuddin, R.; Deris, R.R.R. Chemical Activation of Durian Shell Activated Carbon: Effects of Activation Agents. *Adv. Mat. Res.* **2015**, *1113*, 242–247. [CrossRef]
24. Liu, Y.; Yao, X.; Wang, Z.; Li, H.; Shen, X.; Yao, Z.; Qian, F. Synthesis of Activated Carbon from Citric Acid Residue by Phosphoric Acid Activation for the Removal of Chemical Oxygen Demand from Sugar-Containing Wastewater. *Environ. Eng. Sci.* **2019**, *36*, 656–666. [CrossRef]
25. Wu, H.; Zhang, T.; Pan, R.; Chun, Y.; Zhou, H.; Zhu, W.; Peng, H.; Zhang, Q. Sintering-Free Preparation of Porous Ceramsite Using Low-Temperature Decomposing Pore Former and Its Sound-Absorbing Performance. *Constr. Build. Mater.* **2018**, *171*, 367–376. [CrossRef]
26. Shahrashoub, M.; Bakhtiari, S. The Efficiency of Activated Carbon/Magnetite Nanoparticles Composites in Copper Removal: Industrial Waste Recovery, Green Synthesis, Characterization, and Adsorption-Desorption Studies. *Microporous Mesoporous Mater.* **2021**, *311*, 110692. [CrossRef]
27. Lam, S.S.; Liew, R.K.; Cheng, C.K.; Rasit, N.; Ooi, C.K.; Ma, N.L.; Ng, J.H.; Lam, W.H.; Chong, C.T.; Chase, H.A. Pyrolysis Production of Fruit Peel Biochar for Potential Use in Treatment of Palm Oil Mill Effluent. *J. Environ. Manag.* **2018**, *213*, 400–408. [CrossRef]
28. Ramirez, A.P.; Giraldo, S.; Ulloa, M.; Flórez, E.; Acelas, N.Y. Production and Characterization of Activated Carbon from Wood Wastes. *J. Phys. Conf. Ser.* **2017**, *935*, 012012. [CrossRef]
29. Kamaruddin, M.; Mohd Suffian, Y.; Azmier, M. Optimization of Durian Peel Based Activated Carbon Preparation Conditions for Ammoniacal Nitrogen Removal from Semi-Aerobic Landfill Leachate. *J. Sci. Ind. Res.* **2011**, *70*, 554–560.
30. Kamaruddin, M.A.; Yusoff, M.S.; Ahmad, M.A. Optimization of Preparation Conditions for Durian Peel-Based Activated Carbon for the Removal of COD and Ammoniacal Nitrogen (NH3-N) Using Response-Surface Methodology. *Kuwait J. Sci. Eng.* **2012**, *39*, 37–58.
31. Tey, J.P.; Careem, M.A.; Yarmo, M.A.; Arof, A.K. Durian Shell-Based Activated Carbon Electrode for EDLCs. *Ionics* **2016**, *22*, 1209–1216. [CrossRef]
32. Tham, Y.J.; Latif, P.A.; Abdullah, A.M.; Shamala-Devi, A.; Taufiq-Yap, Y.H. Performances of Toluene Removal by Activated Carbon Derived from Durian Shell. *Bioresour. Technol.* **2011**, *102*, 724–728. [CrossRef] [PubMed]
33. Ismail, A.; Sudrajat, H.; Jumbianti, D. Activated Carbon from Durian Seed by H3PO4 Activation: Preparation and Pore Structure Characterization. *Indo. J. Chem.* **2010**, *10*, 36–40. [CrossRef]
34. Tamjid Farki, N.N.A.N.L.; Abdulhameed, A.S.; Surip, S.N.; ALOthman, Z.A.; Jawad, A.H. Tropical Fruit Wastes Including Durian Seeds and Rambutan Peels as a Precursor for Producing Activated Carbon Using H_3PO_4-Assisted Microwave Method: RSM-BBD Optimization and Mechanism for Methylene Blue Dye Adsorption. *Int. J. Phytoremediat.* **2023**, *25*, 1–12. [CrossRef] [PubMed]
35. Wang, X.; Li, D.; Li, W.; Peng, J.; Xia, H.; Zhang, L.; Guo, S.; Chen, G. Optimization of Mesoporous Activated Carbon from Coconut Shells by Chemical Activation with Phosphoric Acid. *Bioresources* **2013**, *8*, 6184–6195. [CrossRef]
36. Li, Y.; Ding, X.; Guo, Y.; Wang, L.; Rong, C.; Qu, Y.; Ma, X.; Wang, Z. A Simple and Highly Effective Process for the Preparation of Activated Carbons with High Surface Area. *Mater. Chem. Phys.* **2011**, *127*, 495–500. [CrossRef]
37. Lim, W.C.; Srinivasakannan, C.; al Shoaibi, A. Cleaner Production of Porous Carbon from Palm Shells through Recovery and Reuse of Phosphoric Acid. *J. Clean. Prod.* **2015**, *102*, 501–511. [CrossRef]
38. Arshadi, M.; Shakeri, H.; Salvacion, J.W.L. A Green Adsorbent for the Removal of BTEX from Aqueous Media. *RSC Adv.* **2016**, *6*, 14290–14305. [CrossRef]
39. Ahmad, M.A.; Ahmad Puad, N.A.; Bello, O.S. Kinetic, Equilibrium and Thermodynamic Studies of Synthetic Dye Removal Using Pomegranate Peel Activated Carbon Prepared by Microwave-Induced KOH Activation. *Water Resour. Ind.* **2014**, *6*, 18–35. [CrossRef]
40. Demiral, H.; Güngör, C. Adsorption of Copper(II) from Aqueous Solutions on Activated Carbon Prepared from Grape Bagasse. *J. Clean. Prod.* **2016**, *124*, 103–113. [CrossRef]
41. Rattanapan, S.; Srikram, J.; Kongsune, P. Adsorption of Methyl Orange on Coffee Grounds Activated Carbon. *Energy Procedia* **2017**, *138*, 949–954. [CrossRef]

42. Thue, P.S.; Lima, E.C.; Sieliechi, J.M.; Saucier, C.; Dias, S.L.P.; Vaghetti, J.C.P.; Rodembusch, F.S.; Pavan, F.A. Effects of First-Row Transition Metals and Impregnation Ratios on the Physicochemical Properties of Microwave-Assisted Activated Carbons from Wood Biomass. *J. Colloid. Interface Sci.* **2017**, *486*, 163–175. [CrossRef] [PubMed]
43. Belhamdi, B.; Merzougui, Z.; Laksaci, H.; Trari, M. The Removal and Adsorption Mechanisms of Free Amino Acid L-Tryptophan from Aqueous Solution by Biomass-Based Activated Carbon by H_3PO_4 Activation: Regeneration Study. *Phys. Chem. Earth Parts A/B/C* **2019**, *114*, 102791. [CrossRef]
44. Wang, J.; Tang, J. Fe-Based Fenton-like Catalysts for Water Treatment: Preparation, Characterization and Modification. *Chemosphere* **2021**, *276*, 130177. [CrossRef]
45. Aliakbari, Z.; Younesi, H.; Ghoreyshi, A.A.; Bahramifar, N.; Heidari, A. Production and Characterization of Sewage-Sludge Based Activated Carbons Under Different Post-Activation Conditions. *Waste Biomass Valorization* **2018**, *9*, 451–463. [CrossRef]
46. Alam, M.M.; Hossain, M.A.; Hossain, M.D.; Johir, M.A.H.; Hossen, J.; Rahman, M.S.; Zhou, J.L.; Hasan, A.T.M.K.; Karmakar, A.K.; Ahmed, M.B. The Potentiality of Rice Husk-Derived Activated Carbon: From Synthesis to Application. *Processes* **2020**, *8*, 203. [CrossRef]
47. Bakar, N.A.; Othman, N.; Yunus, Z.M.; Altowayti, W.A.H.; Al-Gheethi, A.; Asharuddin, S.M.; Tahir, M.; Fitriani, N.; Mohd-Salleh, S.N.A. Nipah (Musa Acuminata Balbisiana) Banana Peel as a Lignocellulosic Precursor for Activated Carbon: Characterization Study after Carbonization Process with Phosphoric Acid Impregnated Activated Carbon. *Biomass Convers. Biorefin* **2021**, *13*, 11085–11098. [CrossRef]
48. Owkusumsirisakul, J.; Keeriang, T.; Laosiripojana, N.; Issro, C. Investigation on the Effects of Carbonization Parameters on Carbon Material Produced from Durian Shell. *Biomass Convers. Biorefin* **2022**, *12*, 4719–4727. [CrossRef]
49. Saad, M.J.; Chia, C.H.; Zakaria, S.; Sajab, M.S.; Misran, S.; Abdul Rahman, M.H.; Chin, S.X. Physical and Chemical Properties of the Rice Straw Activated Carbon Produced from Carbonization and KOH Activation Processes. *Sains Malays.* **2019**, *48*, 385–391. [CrossRef]
50. Babinszki, B.; Jakab, E.; Sebestyén, Z.; Blazsó, M.; Berényi, B.; Kumar, J.; Krishna, B.B.; Bhaskar, T.; Czégény, Z. Comparison of Hydrothermal Carbonization and Torrefaction of Azolla Biomass: Analysis of the Solid Products. *J. Anal. Appl. Pyrolysis* **2020**, *149*, 104844. [CrossRef]
51. Yuliusman; Ayu, M.P.; Hanafi, A.; Nafisah, A.R. Activated Carbon Preparation from Durian Peel Wastes Using Chemical and Physical Activation. *AIP Conf. Proc.* **2020**, *2230*, 030020.
52. Han, Q.; Wang, J.; Goodman, B.A.; Xie, J.; Liu, Z. High Adsorption of Methylene Blue by Activated Carbon Prepared from Phosphoric Acid Treated Eucalyptus Residue. *Powder Technol.* **2020**, *366*, 239–248. [CrossRef]
53. Sujiono, E.H.; Zabrian, D.; Zurnansyah; Mulyati; Zharvan, V.; Samnur; Humairah, N.A. Fabrication and Characterization of Coconut Shell Activated Carbon Using Variation Chemical Activation for Wastewater Treatment Application. *Results Chem.* **2022**, *4*, 100291. [CrossRef]
54. Singh, C.K.; Sahu, J.N.; Mahalik, K.K.; Mohanty, C.R.; Mohan, B.R.; Meikap, B.C. Studies on the Removal of Pb(II) from Wastewater by Activated Carbon Developed from Tamarind Wood Activated with Sulphuric Acid. *J. Hazard. Mater.* **2008**, *153*, 221–228. [CrossRef] [PubMed]
55. Gupta, H.; Gogate, P.R. Intensified Removal of Copper from Waste Water Using Activated Watermelon Based Biosorbent in the Presence of Ultrasound. *Ultrason. Sonochem.* **2016**, *30*, 113–122. [CrossRef] [PubMed]
56. Yakout, S.M.; Sharaf El-Deen, G. Characterization of Activated Carbon Prepared by Phosphoric Acid Activation of Olive Stones. *Arab. J. Chem.* **2016**, *9*, S1155–S1162. [CrossRef]
57. İzgi, M.S.; Saka, C.; Baytar, O.; Saraçoğlu, G.; Şahin, Ö. Preparation and Characterization of Activated Carbon from Microwave and Conventional Heated Almond Shells Using Phosphoric Acid Activation. *Anal. Lett.* **2019**, *52*, 772–789. [CrossRef]
58. Feng, P.; Li, J.; Wang, H.; Xu, Z. Biomass-Based Activated Carbon and Activators: Preparation of Activated Carbon from Corncob by Chemical Activation with Biomass Pyrolysis Liquids. *ACS Omega* **2020**, *5*, 24064–24072. [CrossRef]
59. Musthapa, S.M.B.H.; Shams, S.; Reddy Prasad, D.M. Removal of Pollutants from Wastewater Using Activated Carbon from Durian Peel. *IOP Conf. Ser. Earth Environ. Sci.* **2023**, *1135*, 012001. [CrossRef]
60. Zakaria, R.; Jamalluddin, N.A.; Abu Bakar, M.Z. Effect of Impregnation Ratio and Activation Temperature on the Yield and Adsorption Performance of Mangrove Based Activated Carbon for Methylene Blue Removal. *Results Mater.* **2021**, *10*, 100183. [CrossRef]
61. Eke-emezie, N.; Etuk, B.R.; Akpan, O.P.; Chinweoke, O.C. Cyanide Removal from Cassava Wastewater onto H_3PO_4 Activated Periwinkle Shell Carbon. *Appl. Water Sci.* **2022**, *12*, 157. [CrossRef]

Disclaimer/Publisher's Note: The statements, opinions and data contained in all publications are solely those of the individual author(s) and contributor(s) and not of MDPI and/or the editor(s). MDPI and/or the editor(s) disclaim responsibility for any injury to people or property resulting from any ideas, methods, instructions or products referred to in the content.